

1 Direct observation for RH-dependent mixing states of submicron 2 particles containing organic surfactants and inorganic salts

3 Chun Xiong^{1#}, Binyu Kuang^{1#}, Fei Zhang¹, Xiangyu Pei¹, Zhengning Xu¹, Zhibin Wang^{1,2,3*}

4 ¹College of Environmental and Resource Sciences, Zhejiang University, Zhejiang Provincial Key Laboratory of Organic
5 Pollution Process and Control, Hangzhou, 310058, China

6 ²ZJU-Hangzhou Global Scientific and Technological Innovation Center, Zhejiang University, Hangzhou 311215, China

7 ³Key Laboratory of Environment Remediation and Ecological Health, Ministry of Education, Zhejiang University, Hangzhou,
8 310058, China

9 *Correspondence to Zhibin Wang (wangzhibin@zju.edu.cn)

10 # Chun Xiong and Binyu Kuang contribute equally to this work.

11 **Abstract:** Aerosol mixing state plays an important role in heterogeneous reactions and CCN activity. Organic surfactants could
12 affect aerosol mixing state through bulk-surface partitioning. However, the mixing state of surfactant containing particles
13 remains unclear due to the lack of direct measurements. Here, direct characterizations of mixing state for 20 kinds of submicron
14 particles containing inorganic salts (NaCl and (NH₄)₂SO₄) and atmospheric organic surfactants (organosulfates,
15 organosulfonates, and dicarboxylic acids) were conducted upon relative humidity (RH) cycling by Environmental Scanning
16 Electron Microscopy (ESEM). As RH increased, surfactant shells inhibited water diffusion exposing to inorganic core, leading
17 to notably increased inorganic deliquescence RH (88.3–99.5%) compared with pure inorganic aerosol. Meanwhile, we directly
18 observed obvious Ostwald ripening process, that is, the growth of larger crystals at the expense of smaller ones, in 6 among
19 10 NaCl-organic surfactants systems. As a result of water inhibition by organic surfactant shell, Ostwald ripening in all systems
20 occurred at RH above 90%, which were higher than reported RH range for pure NaCl measured at 27°C (75–77%). As RH
21 decreased, 8 systems underwent liquid-liquid phase separation (LLPS) before efflorescence, showing a strong dependence on
22 organic molecular oxygen-to-carbon ratio (O:C). Quantitatively, LLPS was always observed when O:C ≤ 0.43 and was never
23 observed when O:C > ~0.57. Separation RH (SRH) of inorganic salt-organic surfactant mixtures generally followed the trend
24 of (NH₄)₂SO₄ < NaCl, which is consistent with their salting out efficiencies reported in previous studies. Solid phase
25 separations were observed after efflorescence for systems without LLPS. Our results provide a unique insight into the
26 consecutive mixing processes of the inorganic salt-organic surfactant particles, which would help improve our fundamental
27 knowledge of model development on radiative effect.

30 Atmospheric particles are complex mixtures of multiple inorganic and organic matters (Pöschl, 2005). When relative
31 humidity (RH) varies, particles can undergo phase transitions such as deliquescence (Peng et al., 2001), efflorescence
32 (Takahama et al., 2007), and liquid–liquid phase separation (LLPS) (Martin, 2000), hence altering mixing state. The transition
33 of aerosol mixing state can influence gas uptake, hygroscopicity, cloud condensation nuclei (CCN) activity, and radiative
34 absorption (Riemer et al., 2019).

35 Upon hydration, previous studies suggested that different mixing state between inorganic and organic matters influence
36 aerosol hygroscopic behaviours (e.g., deliquescence) and solar radiation (Peng et al., 2016; Li et al., 2021). For instance, Peng
37 et al. (2016) observed internal mixed NaCl–oxalic acid deliquesced at 73% RH, being slightly lower than that of pure NaCl
38 (75%) because of the interactions between inorganic and organic matters. However, Li et al. (2021) found a different
39 deliquescence process if ammonium sulfate (AS) was coated by secondary organic aerosol, the organic shell firstly dissolved
40 at ~50% RH but water uptake of the AS core was inhibited, leading to a higher deliquescence RH of AS (~83–90%). By
41 cryogenic transmission electron microscopy (cryo–TEM), Zhang et al. (2022) directly observed collected particles from a rural
42 site remained LLPS (inner inorganic phase and outer organic phase) between organic matter and inorganic salts when RH
43 raised to $75 \pm 2\%$ and $86 \pm 2\%$, but LLPS disappeared when RH increased to $95 \pm 2\%$. They later suggested that LLPS with
44 higher ratio of organic coating thickness to black carbon size can drive black carbon from inorganic core to organic particle
45 coatings, which could result in 18% radiative absorption overestimation of black carbon aerosols in climate models by
46 assuming a core-shell particle structure.

47 Upon dehydration, phase separation has been frequently observed in ambient particles (You et al., 2012; Ting et al., 2018;
48 Zhang et al., 2020; Zhang et al., 2022). For example, LLPS occurred at $> 90\%$ RH for particles containing water extraction of
49 collected atmospheric particles in Atlanta and simulations indicated that LLPS can decrease particle uptake of N_2O_5 thus
50 increase concentrations of gas–phase NO_3 and N_2O_5 (You et al., 2012). Factors contributing to LLPS, e.g. oxidation levels
51 (Bertram et al., 2011; Song et al., 2017; Song et al., 2019), organic fraction (Ciobanu et al., 2009; Song et al., 2012a), inorganic
52 species (You et al., 2013), and temperature (You and Bertram, 2015; Roy et al., 2020) have been discussed for some specific
53 inorganic–organic or organic–organic systems in literature. Song et al. (2012b) and You et al. (2013) found LLPS always
54 occurred for $\text{O}:\text{C} < \sim 0.5$, never occurred for $\text{O}:\text{C} > 0.8$, and when $\text{O}:\text{C}$ was between 0.5 and 0.8, LLPS was depended on
55 inorganic species. Organic fraction showed controversial effects on LLPS (Bertram et al., 2011; Song et al., 2012a) since
56 Bertram et al. (2011) found a weak effect of organic fraction on LLPS for 8 out of 11 AS–organic systems but the rest systems
57 exhibited a quantifiable dependence of separation RH (SRH) on organic fraction. You et al. (2013) reported SRH among out
58 of 20 organics generally followed the trend of $(\text{NH}_4)_2\text{SO}_4 \geq \text{NH}_4\text{HSO}_4 \geq \text{NaCl} \geq \text{NH}_4\text{NO}_3$, which is consistent with
59 inorganic salting out efficiencies. Temperature did not strongly affect SRH between 253–290 K for AS–organics (O'Brien et
60 al., 2015; You and Bertram, 2015) and NaCl–organics systems (Roy et al., 2020). Recently, dry rate (Altaf and Freedman,

61 2017; Altaf et al., 2018) and size effect (Freedman, 2020; Ott and Freedman, 2021; Ohno et al., 2023) on LLPS were found
62 for submicron particles. Undergoing drying by fast rate ($\sim 27\%$ per minute), phase separation of AS-pimelic acid system
63 occurred in larger particles (75 \sim 322 nm diameter), but smaller particles (below 25 \sim 135 nm diameter) were homogeneous. In
64 slow drying rates (0.04 to 0.08% RH per second), particles with diameter below 43 nm were homogeneous but larger particles
65 (28 \sim 629 nm) were mainly phase-separated (Altaf and Freedman, 2017). Freedman (2020) further explained that LLPS is
66 scarcely occurred in smaller particles as smaller particles cannot overcome the energy barrier needed to form a new phase.

67 Dicarboxylic acids (Ruehl and Wilson, 2014), organosulfates (Bruggemann et al., 2020; Reed et al., 2022), and
68 organosulfonates (Bruggemann et al., 2020; Guo et al., 2020) are important organic constituents in secondary organic aerosol.
69 Primary emission and secondary transition were major sources of dicarboxylic acids and their mass contribution of
70 dicarboxylic acids to total particulate carbon exceeds 10% (Römpp et al., 2006; Ho et al., 2010; Hyder et al., 2012).
71 Organosulfates and organosulfonates, as significant reservoirs of sulfur, comprise an estimated 5%–30% of the total organic
72 aerosol mass (Tolocka and Turpin, 2012; Reed et al., 2022). Above mentioned organics contain both hydrophilic (e.g., sulfo
73 group) and hydrophobic groups (e.g., alkyl group), showing surface activity and causing bulk–surface partitioning (Noziere,
74 2016; Ruehl et al., 2016), hence affecting individual aerosol morphology (Kwamena et al., 2010). However, mixing state of
75 submicron inorganic salt–organic surfactant particles remain unclear due to the lack of direct measurements. Here, we directly
76 observed mixing states of submicron particles containing inorganic salt and organic surfactant with varying organic volume
77 fraction (OVF) upon humidity cycling by Environmental Scanning Electron Microscopy (ESEM). Our results could provide
78 unique insights into the dynamic evolution of inorganic salt–organic surfactant particles under fluctuating atmospheric
79 conditions.

80 **2 Materials and Methods**

81 **2.1 Chemicals**

82 NaCl and AS were purchased from Sinopharm chemical reagent (purity $\geq 99.8\%$) and Sigma Aldrich (purity $\geq 99\%$),
83 respectively. The studied organic substances include 10 surface active organics (five organosulfonates, three organosulfates
84 and two dicarboxylic acids). The five organic sulfonates were sodium propane sulfonate ($C_3H_7SO_3Na$), sodium butane
85 sulfonate ($C_4H_9SO_3Na$), sodium pentane sulfonate ($C_5H_{11}SO_3Na$), sodium heptane sulfonate ($C_7H_{15}SO_3Na$), sodium octane
86 sulfonate ($C_8H_{17}SO_3Na$). The three organic sulfates were sodium methyl sulfate (CH_3SO_4Na), sodium ethyl sulfate
87 ($C_2H_5SO_4Na$) and sodium octyl sulfate ($C_8H_{17}SO_4Na$). Two dicarboxylic acids were pimelic acid (PA) and phenylmalonic acid
88 (PhMA). Relevant properties of used chemicals were summarized in **Table 1**. These organic surfactants were of various
89 solubilities, from sparingly soluble (e.g., 0.07 mol L^{-1} for $C_8H_{17}SO_4Na$) to highly soluble (e.g., 2.6 mol L^{-1} for CH_3SO_4Na).
90 O:C ratios were from 0.38 to 4, covering most of the molar ratios in the atmosphere (0.1–1.0) (You et al., 2013). The studied

91 organic substances contain functional groups such as sulfonates, sulfates, carboxylic acids and aromatics, which were
92 universally detected in atmospheric aerosol samples (Takahama et al., 2007).

93

94

Table 1 Organic surfactants and their relevant properties investigated in this study.

Species	Compounds	Formula	*Solubility (mol L ⁻¹)	O:C	Purity	Supplier
Organic sulfonate	Sodium propane sulfonate	C ₃ H ₇ SO ₃ Na	2.5	1.00	>98%	Aladdin
	Sodium butane sulfonate	C ₄ H ₉ SO ₃ Na	2.4	0.75	≥99%	Aladdin
	Sodium pentane sulfonate	C ₅ H ₁₁ SO ₃ Na	0.8	0.60	98%	Aladdin
	Sodium heptane sulfonate	C ₇ H ₁₅ SO ₃ Na	0.6	0.43	98%	Macklin
	Sodium octane sulfonate	C ₈ H ₁₇ SO ₃ Na	0.07	0.38	≥99%	Macklin
Organic sulfate	Sodium methyl sulfate	CH ₃ SO ₄ Na	2.6	4.00	98%	Energy Chemical
	Sodium ethyl sulfate	C ₂ H ₅ SO ₄ Na	1.5	2.00	98%	Meryer
	Sodium octyl sulfate	C ₈ H ₁₇ SO ₄ Na	0.2	0.50	99%	Rhawn
Dicarboxylic acid	Pimelic acid (PA)	C ₇ H ₁₂ O ₄	0.3	0.57	99%	Macklin
	Phenylmalonic acid (PhMA)	C ₉ H ₈ O ₄	0.2	0.44	98%	Aladdin

95

96 * <https://comptox.epa.gov/> (last access: 19 Jun, 2023)

97 2.2 Aerosol generation and collection

98 The process of aerosol generation and collection was detailedly described by Xiong et al. (2022). In brief, particles were
99 nebulized from solutions of organic and inorganic matters (~5 g L⁻¹) mixed with deionized water (Millipore, resistivity = 18.2
100 MΩ). After drying (RH < 15%) by a silica-gel diffusion dryer, particles were deposited with an eight stage non-viable particle
101 sizing sampler (Models BGI20800 Series, BGI Incorporation) onto 400 mesh copper grids coated with carbon films
102 (Zhongjingkeyi Films Technology Co. Ltd.). Copper grids were mounted on the 7th stage, selecting particles with aerodynamic
103 size of 0.7–1 μm. Collected samples were stored under dry condition (RH < 10%) and were immediately characterized within

104 24 hours to avoid possible sample aging.

105 **2.3 Mixing state observation**

106 Optical microscopy (Ciobanu et al., 2009; Bertram et al., 2011; Song et al., 2012a, b; You et al., 2013), microfluidic device
107 (Roy et al., 2020), Cryo-TEM (Veghte et al., 2014; Freedman, 2020; Ott and Freedman, 2021; Ott et al., 2021; Zhang et al.,
108 2022), ESEM (O'Brien et al., 2015), optical tweezer (Stewart et al., 2015; Tong et al., 2022) and F-AFT (Fluorescence aerosol
109 flow tube) (Ohno et al., 2021; Ohno et al., 2023) were reported methods for detecting aerosol mixing state in the literature.
110 Optical microscopy and microfluidic device were commonly used direct method for substrate-supported droplets but was
111 limited by size range (at least dozens of micrometers). Optical tweezer and F-AFT could investigated LLPS in a levitated
112 micrometer and sub-micrometer droplet, respectively, but are indirect ways, although no distinct differences when comparing
113 to substrate-supported droplets (Ohno et al., 2023). Cryo-TEM and ESEM could detect mixing state in sub-micrometer scale
114 but damage caused by electron beam may exist (depend on chemistry and beam parameters settings). Ott et al. (2021) give
115 some useful suggestions in minimize the damage, e.g., decreasing exposure dose and time to particles.

116 Mixing state was observed by Environmental Scanning Electron Microscopy (ESEM, Thermo Quattro S) with a
117 temperature-controlled stage. The RH in chamber was varied between 0.1 to ~ 25 °C, and controlled by adjusting the
118 temperature (± 0.1 °C) at a predefined pressure (610 Pa). In each experiment, particles with lateral dimensions of ~ 1 μm were
119 selected first (based on the deposition, volume-equivalent size was smaller than 1 μm). Then the RH raised from low ($\sim 30\%$)
120 to high condition ($\sim 100\%$) at the change rate of $2\text{--}3\%$ RH min^{-1} . High RH lasted for at least 5 minutes for equilibrium,
121 promising complete dissolution (O'Brien et al., 2015). With increased RH, most selected particles grew larger to several
122 micrometers before subsequent LLPS experiment. Then, RH decreased to dry condition at similar change rate. Negligible
123 influence on the LLPS of AS-organic (O'Brien et al., 2015; You and Bertram, 2015) and NaCl-organic systems (Roy et al.,
124 2020) in micrometre scale (from several micrometers to dozens of micrometers). Cloud parcel modelling suggests that
125 atmospheric RH fluctuations typically occur from 0 to 3.6% min^{-1} (Pöhlker et al., 2014). Therefore, we assume that the water
126 uptake in our experiments approximates atmospheric conditions (Shiraiwa et al., 2013). Images of mixing states during the
127 whole RH period were acquired at an electron acceleration voltage of 30 kV. The detector used for the ESEM imaging was a
128 scanning transmission electron detector. The images were recorded with line scanning rates of $3\text{--}5$ μs to minimize the possible
129 beam damage (Supporting information, O'Brien et al., 2015). The varying range of RH value between two consecutive pictures
130 were mostly $0.2\text{--}0.4\%$ RH (very narrow), in order to capture the possible quick transitions of mixing states. Each image in our
131 study contained at least 5 particles (or droplets) to ensure the ESEM reproducibility and decrease the uncertainty. In addition,
132 we have repeated some of the experiment (e.g., in the RH decreasing period) for reproducibility validation, and the results
133 showed good consistence (**Fig. S1**).

135 **3.1 Mixing states upon hydration**

136 Deliquescence RH (DRH) and Efflorescence RH (ERH) of pure NaCl (**Fig. 1a–d** and **Fig. S2a–b**) and AS particles (**Fig.**
137 **2a–d** and **Fig. S2c–d**) were firstly tested via the experimental setup. DRH of NaCl and AS were observed at $80.9 \pm 0.1\%$
138 (literature: $77 \pm 1\%$ (Pöhlker et al., 2014)) and $82.1 \pm 0.6\%$ (literature: 82.0% (Onasch et al., 1999)). ERH of NaCl and AS
139 were $48.3 \pm 0.4\%$ (literature: $48 \pm 2\%$ (Zeng et al., 2014)) and $30.7 \pm 0.9\%$ (literature: $31 \pm 1\%$ (Cheng and Kuwata, 2023)).
140 Generally, the experimental DRH and ERH values correspond well with those in literature, confirming the reliability of the
141 experimental setup. DRH of NaCl showed slight deviation by about nearly 4%, which could be explained by kinetic effects
142 when the system had not reached full equilibrium (Pöhlker et al., 2014). Before deliquescence, the substrate-supported NaCl
143 and AS particles both showed substantial water uptake, forming an aqueous halo around a solid core. Similar observational
144 results of NaCl and AS have been reported, and could be explained by interactions at the sample/substrate interface, which
145 plays an important role in such gradual phase transition as additional energy term (Wise et al., 2008; Pöhlker et al., 2014).

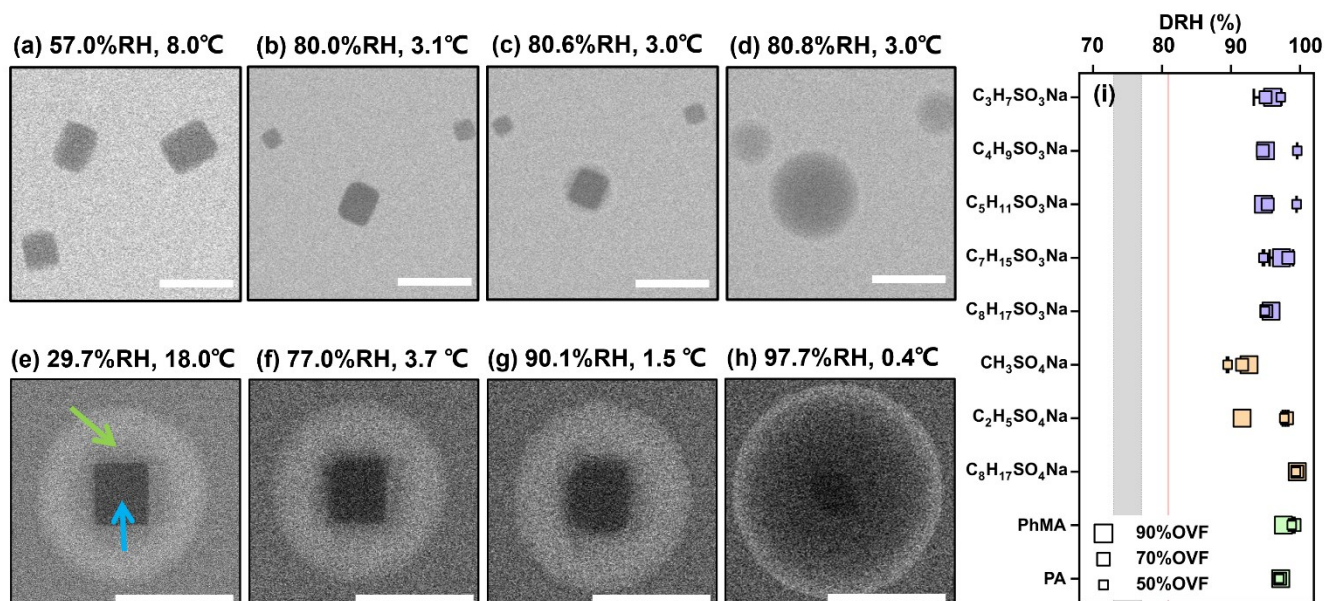
146 **Figure 1e** and **Fig. 2e** illustrate the two separated phases with dark core (blue arrow) and bright shell (green arrow) of
147 dry deposited NaCl–C₂H₅SO₄Na and AS–C₂H₅SO₄Na particles. The dark cores are indicated to be inorganics, because darker
148 regions are characteristic of areas with higher atomic number elements (e.g., Cl) and/or a thicker sample region (Laskin et al.,
149 2006; O'brien et al., 2015). Phase separations with core–shell structure were observed for all studied inorganic salt–organic
150 surfactant systems. This may be attributed to the size range of particles we investigated ($\sim 1 \mu\text{m}$ with dry lateral dimension),
151 since inorganic salt–organic surfactant particles with such size range might overcome the energy barrier needed to form a new
152 phase (Altaf and Freedman, 2017; Altaf et al., 2018; Freedman, 2020; Ott and Freedman, 2021). According to results in
153 Freedman (2020), morphology of most systems were found size-dependent, where large particles were phase-separated and
154 small particles were homogeneous. Furthermore, all systems (e.g. AS–PA and AS–succinic acid systems) with dry diameters
155 larger than $0.7 \mu\text{m}$ were observed phase-separated no matter the occurrence of size dependence (Altaf and Freedman, 2017).
156 Freedman (2020) expected that phase-separation could be attributed by nucleation and growth, therefore larger particles tended
157 to be phase-separated morphology. In another study, Ohno et al. (2021) also found that LLPS occurred at lower RH in smaller
158 droplet (70 – 190 nm) than in larger droplet (260 – 370 nm).

159 When RH increased from dry, as organic phase slowly absorbed water, NaCl and AS cores were not fully dissolved at
160 RH of 90.1% and 91.7% (**Fig. 1g** and **Fig. 2g**), respectively, being notably higher than their DRH. The phenomenon was found
161 for all NaCl–organic surfactant and AS–organic surfactant systems and the DRH of the inorganic salts were ranged in
162 88.3–99.5% (**Fig. 1i** and **Fig. 2i**). Laskina et al. (2015) measured the DRH of pure AS and NaCl at submicrometer (100 nm)
163 and supermicrometer (3–10 μm) size ranges by hygroscopic tandem differential mobility analyzers (HTDMA) and
164 MicroRaman Spectroscopy, respectively, and the deviations between them were both within 3%, indicating that DRH of pure
165 AS and NaCl showed weak size dependence ($> 100 \text{ nm}$). In addition, Cheng and Kuwata (2023) used low-temperature

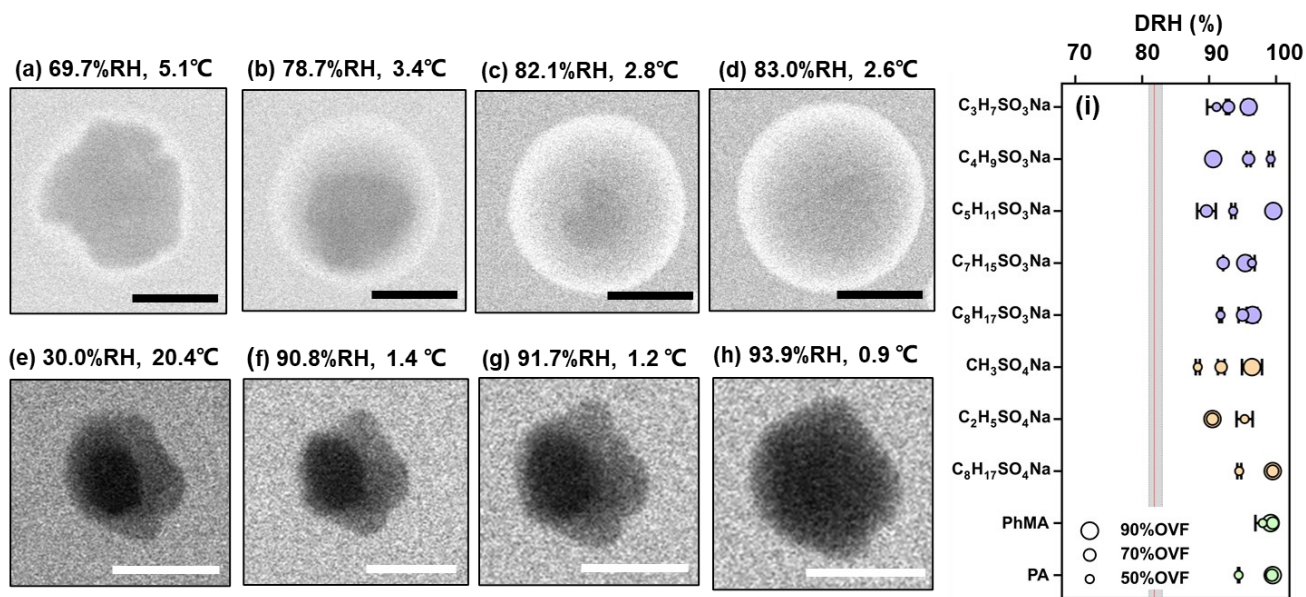
166 hygroscopicity tandem differential mobility analyzer (Low-T HTDMA) and observed consistent DRH of NaCl and AS within
167 experimental error under temperature ranged in $-10\text{ }^{\circ}\text{C}$ to $22.5\text{ }^{\circ}\text{C}$, suggesting that the DRH of NaCl and AS experience a
168 neglect temperature dependence. According to the above-mentioned studies, DRH of pure AS and NaCl displayed weak
169 dependence on size ($> 100\text{ nm}$) and temperature, and we therefore concluded that surfactant shell inhibits water diffusion
170 exposing to inorganic cores, resulting in delays of deliquescence of inorganic cores. The inhibition of surfactant shell could be
171 triggered by increased viscosity with raised RH, since reported studies have reported that organic shells can transform from
172 solid to semisolid with high viscosity at wet condition (Zhang et al., 2018). In a RH-constrained lab study at constant room
173 temperature, Li et al. (2021) also observed organic coating of secondary organic aerosol (oxidizing α -pinene) started to
174 deliquesce first, but the phase changes of AS cores from solid to liquid took place at 83–90% RH, lower than those in the
175 current study. This was possibly caused by the water diffusion coefficient through organic phase, which could be affected by
176 organic species and environment parameters such as temperature. Given by Nguyen et al. (2017), the diffusion coefficient of
177 a water molecule through an organic shell could be decreased by lower temperature. In the current study, higher RH in the
178 ESEM chamber was achieved by decreasing temperature, thus might decrease diffusion coefficient of water in organic
179 surfactant and lead to higher DRH than those in Li et al. (2021). Previous study and the current work indicated the phenomenon
180 (water inhabitation by organic coating) to be a common and important procedure in affecting ambient aerosol hygroscopicity,
181 because inorganic–organic core–shell structures were ubiquitous observed in field (Li et al., 2016; Unga et al., 2018; Xu et al.,
182 2020; Li et al., 2021; Wang et al., 2021; Zhang et al., 2022). Though the water inhabitation of organic shell in the current study
183 was observed at temperature much lower than room temperature, it is meaningful and may affect aerosol properties in some
184 special area such as polar regions (Lambert et al., 2013; Kirpes et al., 2022; Zavacka et al., 2022) or winter time period (Xu et
185 al., 2021; Zhang et al., 2021) where are characteristic with low-temperature environment.

186 As previous study believed that deliquescence on hydration for inorganics independent of circumstances, **Fig. 3** illustrates
187 an unexpected phase transition of NaCl cores coated with $\text{C}_2\text{H}_5\text{SO}_4\text{Na}$. As shown in **Fig. 3a**, a droplet with several NaCl cores
188 was observed at 97.0% RH since discussed above that organic shell inhibits water diffusion. NaCl cores in droplet were a
189 bigger one (marked by white square) and the rest were smaller. When RH gradually raised (**Fig. 3b–c**), as smaller NaCl cores
190 serially deliquesced and dissolved, the size of the bigger NaCl core surprisingly increased, indicating a simultaneous NaCl
191 recrystallization at the expense of smaller ones (i.e., Ostwald ripening) (Boistelle and Astier, 1988). After other small particles
192 totally dissolve, the bigger NaCl core deliquesced and fully dissolved at 99.5% RH (**Fig. 3d**). A previous study reported
193 “efflorescence upon hydration” for 1:1 mixed NaCl-gluconic acid and AS-gluconic acid by optical tweezer (Zhu et al., 2022).
194 Based on IR spectrum, they found the coexistence of partial efflorescence mixed state, ultraviscous state and liquid state during
195 “efflorescence upon hydration” period, indicating an unstable crystal and concentrated liquid state of NaCl. In this
196 circumstance, Ostwald ripening can take place. Ostwald ripening was triggered by the decrease of total system free energy,
197 since dissolved small and effloresced big crystals reduce the total system free energy (Voorhees, 1985). We directly and
198 observed obvious Ostwald ripening processes in 6 among 10 NaCl–organic surfactants systems. As a results of water inhibition

199 by surfactant shell discussed above, Ostwald ripening here all occurred at RH above 90%, which were notably higher than
 200 reported 75%–77% for pure NaCl measured by X-ray microspectroscopy at 27°C (Pöhlker et al., 2014).
 201

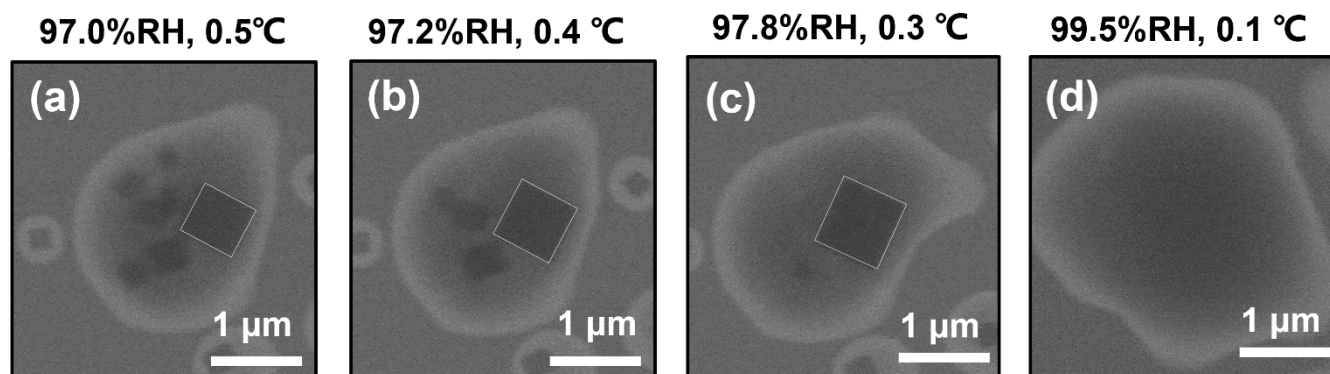


202 **Figure 1.** ESEM images of (a–d) pure NaCl and (e–h) NaCl–C₂H₅SO₄Na (70% OVF) with different RH. Blue and green
 203 arrows indicate the inorganic phase and organic phase, respectively. The RH value that NaCl core fully dissolved (DRH) for
 204 NaCl–organic surfactant systems with different OVF (i). Grey area in (i) covers DRH range of NaCl in the literature obtained
 205 from Peng et al. (2022). Red line indicates the measured average DRH of pure NaCl (80.9 ± 0.1%). Scale bars in (a–h) were 1
 206 μm.
 207
 208

210
211

212 **Figure 2.** ESEM images of (a–d) pure AS and (e–h) AS–C₂H₅SO₄Na (50% OVF) with different RH. Blue and green arrows
 213 indicate the inorganic phase and organic phase, respectively. The RH value that AS core fully dissolved (DRH) for AS–organic
 214 surfactant systems with different OVF (i). Grey area in (i) covers DRH range of AS in the literature obtained from Peng et al.
 215 (2022). Red line indicates the measured average DRH of pure AS (82.1 ± 0.6%). Scale bars in (a–h) were 1 μm.

216



218

219 **Figure 3.** ESEM images of Ostwald ripening for NaCl-C₈H₁₇SO₄Na (50% OVF) particle. White square indicates the biggest
220 NaCl core (assumed square) in droplet. The biggest NaCl grew larger (recrystallization) while the small NaCl cores dissolved.

221

222 3.2 Mixing states upon dehydration

223 LLPS

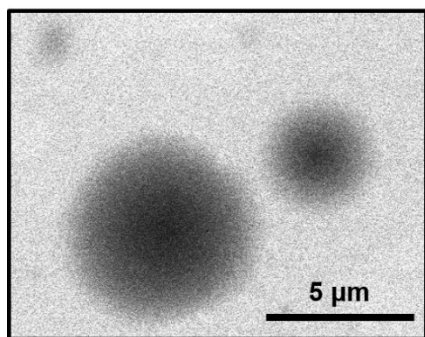
224 In **Fig. 4a**, AS-C₈H₁₇SO₄Na was homogeneous under RH of 99.5%. When RH decreased to 99.1%, the particles showed
225 two separated liquid phases (i.e., LLPS) with a dark inner phase and a light outer phase (**Fig. 4b**), which were highlighted by
226 the blue and green arrows. In addition, the AS-C₈H₁₇SO₄Na remained LLPS when RH continue to decline until efflorescence
227 of inner inorganic phase occurred (**Fig. 4c**). In our study, 8 among 20 chemical systems underwent LLPS, including 4
228 AS-organic surfactant systems and 4 NaCl-organic surfactant systems. **Fig. 5** illustrates the relationship between LLPS
229 occurrence and molar ratios (O:C and H:C) of the surface-active organics, as well as reported results of other binary inorganic
230 salt-organic systems in literature (Bertram et al., 2011; You et al., 2013; You and Bertram, 2015). In our study, LLPS always
231 occurs when the O:C ratio is below 0.43 (yellow dashed line in **Fig. 5**) for NaCl-organic surfactant and AS-organic surfactant
232 droplets. This value was close to the reported values in You et al. (2013) (~ 0.5). However, in their results, LLPS was never
233 observed when O:C was above ~ 0.8 (grey dashed line in **Fig. 5**) (Bertram et al., 2011; Song et al., 2012b; You et al.,
234 2013), which was higher than that in our experiment (0.57). We ascribe this to the insufficient chemical systems in our
235 experiment (10 systems), which was notably smaller than in previous studies (over 30). As a result, the bounds of O:C
236 determining LLPS were not changed if our results were added in previous studies such as You et al. (2013) and Song et al.
237 (2012b).

238 In order to analyze the effect of inorganic salts in LLPS, we compared SRH of systems which contained same organic
239 matters but different inorganic salts. Results showed that SRH of AS-C₈H₁₇SO₄Na (70% OVF), AS-C₈H₁₇SO₃Na (90% OVF),
240 AS-PhMA (90% OVF) and AS-PA (90% OVF) were $98.7 \pm 0.5\%$, $81.3 \pm 1.2\%$, $97.9 \pm 1.0\%$ and $98.5 \pm 0.8\%$, and were all
241 notably higher than SRH of corresponding NaCl-containing systems ($92.5 \pm 3.9\%$, $56.4 \pm 1.2\%$, $85.6 \pm 3.6\%$ and $66.7 \pm 0.8\%$),
242 respectively. This was attributed to different salting out efficiency of inorganic salts, since You et al. (2013) found the SRH of
243 inorganic-organic mixtures followed the trend of $(\text{NH}_4)_2\text{SO}_4 \geq \text{NH}_4\text{HSO}_4 \geq \text{NaCl} \geq \text{NH}_4\text{NO}_3$, which were generally consistent
244 with their salting out efficiency.

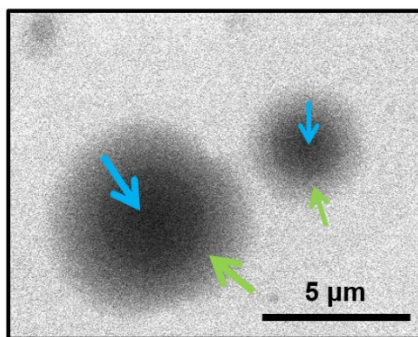
245 The measured SRH values as a function of OVF are plotted in **Fig. 6**. AS-C₈H₁₇SO₄Na showed SRH of $98.7 \pm 0.5\%$
246 when OVF was 70%, higher than those of 50% OVF ($82.1 \pm 1.6\%$) and 90% OVF ($80.0 \pm 0.9\%$). However, the phenomenon
247 was totally different from that of AS-C₈H₁₇SO₃Na, which showed lower SRH with 70% OVF ($62.2 \pm 2.6\%$) than those of 50%
248 OVF ($69.6 \pm 1.0\%$) and 90% OVF ($81.3 \pm 1.2\%$). Therefore, the above results indicated controversial effect of OVF on SRH
249 (Bertram et al., 2011; Song et al., 2012a).

250

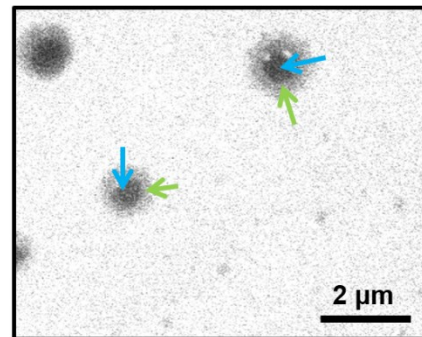
(a) 99.5%RH, 0.1 °C



(b) 99.1%RH, 0.2 °C



(c) 30.8%RH, 17.4 °C



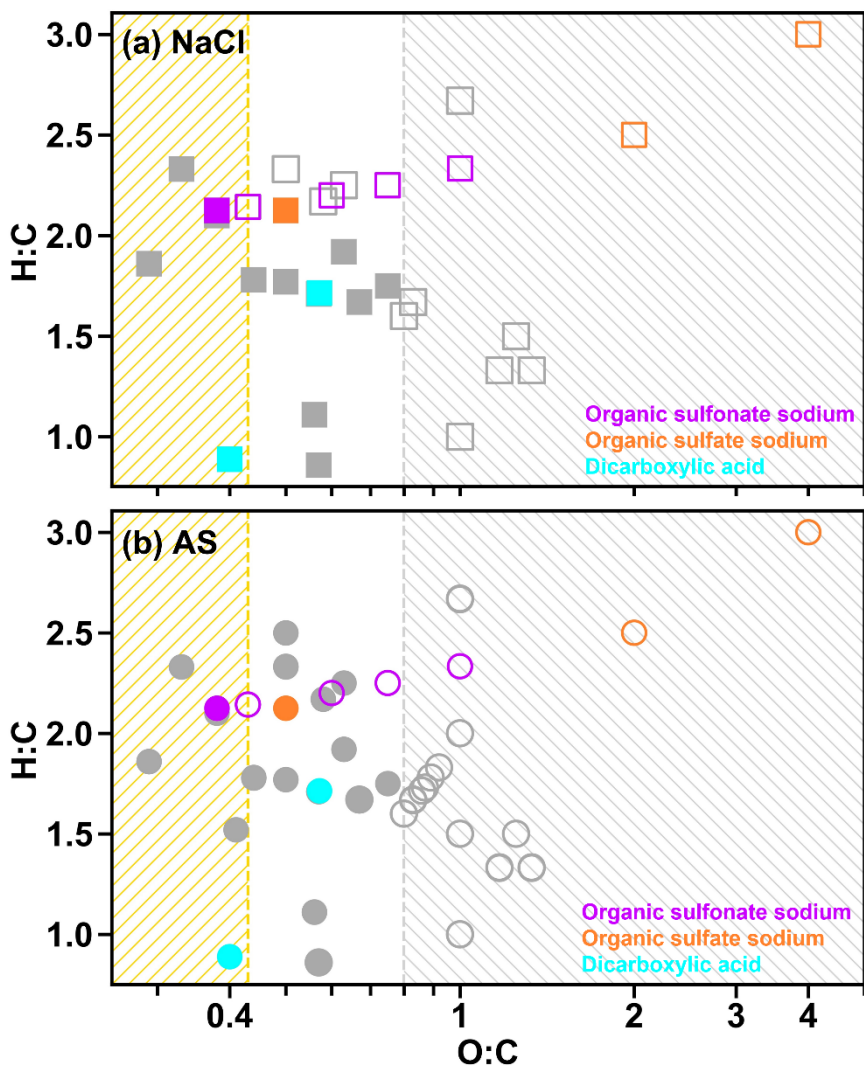
251

252

253

Figure 4. ESEM images of (a) homogeneous AS-C₈H₁₇SO₄Na particles (70% OVF) underwent (b) LLPS and (c) efflorescence.

254



255

256

257

258

259

260

261

Figure 5. Van Krevelen Diagram for the mixed inorganic–surfactants particles in the current study (symbols in red, orange and cyan): (a) NaCl–organic surfactant and (b) AS–organic surfactant systems. Solid symbols indicate that LLPS was observed for particles with at least one OVF, while hollow symbols indicate that LLPS was not observed for particles with all OVFs. Symbols in grey in (a) and (b) were results obtained from Bertram et al. (2011), You et al. (2013) and You and Bertram (2015). Yellow-hatched region ($O:C < 0.43$) means that LLPS observed in all investigated systems, while grey-hatched region ($O:C > 0.8$) means no LLPS detected in any of the investigated systems.

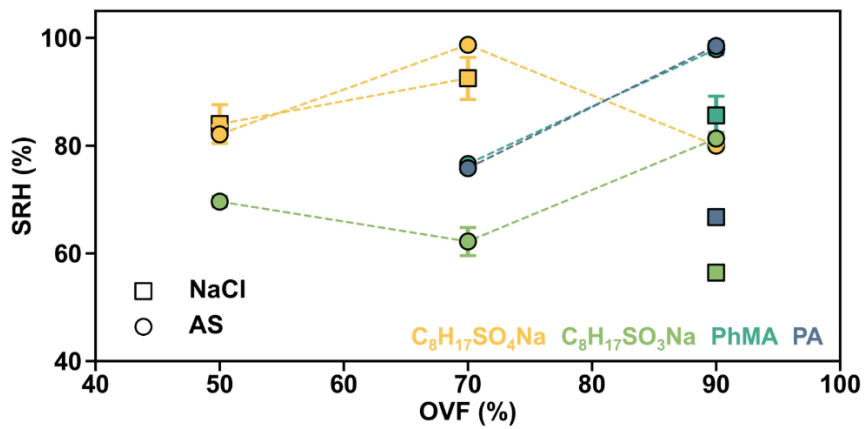


Figure 6. Summary of SRH results as a function of OVF for inorganic-surfactant particles.

262
263
264

265 **Solid phase separation**

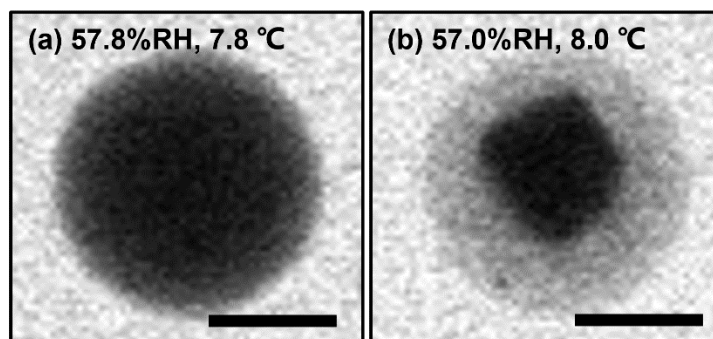
266 For mixed systems without undergoing LLPS, we found they were separated with distinct core-shell phases from
267 homogeneous morphology at low RH. However, this phase transition was different from LLPS, since the inner phase was with
268 irregular shape (LLPS occurred with rounded inner liquid phase), which was attributed to the efflorescence progress of
269 inorganic salt (**Fig. 7**). Therefore, we termed it solid phase separation. The efflorescence RH (ERH) of inner inorganic salt,
270 therefore, was the solid phase separation RH.

271 In **Fig. 8a**, ERH of NaCl-organic surfactant particles with 50%, 70% and 90% OVF were ranged in 47.0–61.8%, which
272 was higher than the measured ERH ($48.3 \pm 0.4\%$) and reported ERH range of pure NaCl (41–51%) (Peng et al., 2022). This
273 could be explained by the interaction between organic and inorganic matters. For example, Ghorai et al. (2014) found an acid
274 displacement reaction in NaCl-glutaric acid systems, which was driven by gaseous HCl liberation and causing chloride
275 depletion. Such interactions of chloride depletion may facilitate efflorescence transitions, resulting in efflorescence at ~ 68%
276 RH and ~ 60% RH, respectively, for internally mixed NaCl-glutaric acid particles with molar ratios of 1:3 and 1:1. Higher
277 ERH could also be attributed to heterogeneous nucleation initiated by chemical purities (Choi and Chan, 2002). Choi and Chan
278 (2002) observed 54.4% ERH for a 1:1 mixed NaCl-glutaric acid, and they explained that insoluble additives crystallized and
279 formed nuclei for the heterogeneous efflorescence of inorganic salts, leading to their higher ERH values.

280 As for AS-organic surfactant systems (**Fig. 8b**), efflorescence was observed for 27 among 30 aerosol samples. We did
281 not observe distinct occurrence of efflorescence for the rest 3 samples, and 2 samples among 3 were with 90% OVF, which
282 could be explained by the possible loss of AS when it was persistently exposed to electronic beam (Posfai et al., 2013; O'Brien
283 et al., 2015), especially for particles in which inorganic fractions were small (i.e., high OVF). ERH values of AS-organic
284 surfactant particles with 50%, 70%, and 90% OVF ranged in 31.2–46.6%, showing a close result to the reported ERH of pure
285 AS (30–48%) (Peng et al., 2022), but higher than the measured ERH ($30.7 \pm 0.9\%$). The potential cause may be the
286 heterogeneous crystallization of AS on organic salts (Wang et al., 2019; Yang et al., 2019; Ma et al., 2021). For example, Wang
287 et al. (2019) investigated the efflorescence of AS in AS-sodium oxalate and found SRH values were 48.9% and 55.3% with
288 organic-inorganic mole ratios of 1:1 and 3:1, respectively, which were higher than that of pure AS (47.5%). Likely, Yang et al.
289 (2019) also observed that the initial ERH of AS rose to 47.7% and 62% for inorganic mole ratios 1:3 and 1:1 AS-sodium
290 pyruvate mixtures, respectively.

291

NaCl-PhMA (50%OVF)



AS-CH₃SO₄Na (90%OVF)

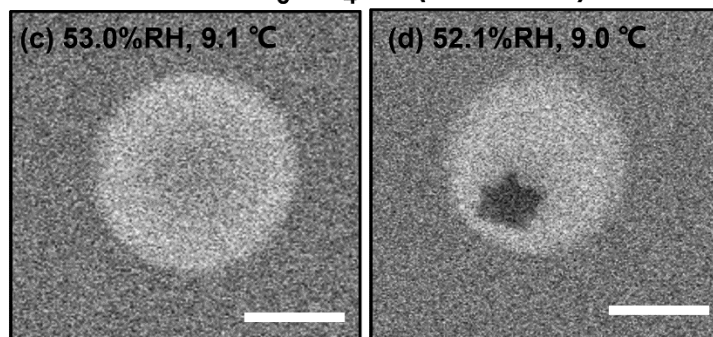
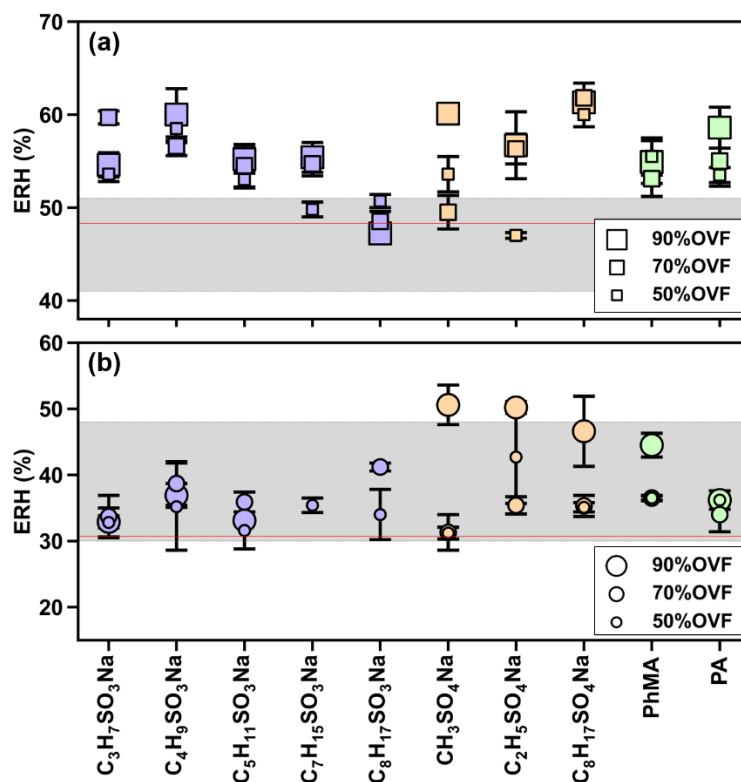


Figure 7. ESEM images of solid phase separation for (a–b) NaCl–PhMA and (c–d) AS–CH₃SO₄Na systems. The scale bars in (a–d) were 500 nm.

292
293
294
295



297

298

299

300

301

Figure 8. Measurements of efflorescence relative humidity (ERH) of (a) NaCl-organic surfactant and (b) AS-organic surfactant particles. The grey areas in (a) and (b) indicate the efflorescence RH range of NaCl (41–51%) and AS (30–48%) obtained from Peng et al. (2022). Red lines in (a) and (b) represent the measured average ERH of pure NaCl ($48.3 \pm 0.4\%$) and AS ($30.7 \pm 0.9\%$).

302

3.3 Atmospheric implication

303

304

305

306

307

308

309

310

311

Dicarboxylic acids, organosulfates, and organosulfonates are important surface-active organic constituents in secondary organic aerosol. Few studies comprehensively studied their mixing state upon fluctuating RH cycling, which is a simulate of real atmospheric condition. In this work, we concluded that mixing state affected interactions of inorganic salt with water. Since common assumptions in chemical transport models (including ISORROPIA-II (Fountoukis and Nenes, 2007), EQSAM (Metzger et al., 2002a; Metzger et al., 2002b), and MOSAIC (Zaveri et al., 2008)) are that water uptake is determined separately by the inorganic compounds and organics (i.e., the effect of mixing state was ignored) (Myhre et al., 2007; Nandy et al., 2021), thereby our results implied further effect of mixing states on estimations of aerosol hygroscopicity (e.g., growth factor), optical properties, and radiative forcing.

During dehydration, we investigated phase-separated before and after efflorescence for inorganic salts-organic surfactant

312 particles. Compared with homogeneous particles, phase-separated particles could decrease trace gas uptake (You et al., 2012),
313 resulting in reduction of the formation of secondary organic aerosols (SOAs) (Zhang et al., 2018). In addition, organic phase
314 was enriched in “outer shell”, which can potentially alter aerosol water activity and lower aerosol surface tension, hence
315 affecting aerosol–cloud interactions because water uptake of organic matter in current models (e.g. MPMPO (Griffin et al.,
316 2003) and SOA treatment in CMAQ v5.2 (Pye et al., 2017)) is estimated by highly parameterized relationships assuming ideal
317 solutions, e.g., using the kappa hygroscopicity parameter with water surface tension (Petters and Kreidenweis, 2007; Nandy
318 et al., 2021).

319 Our results provide comprehensive information of mixing states between inorganic salts and organic surfactant in
320 nanoscale perspective, which could help the establishment of incorporation atmospheric modeling, to improve predictions on
321 indirect effects of aerosol–climate interactions. We should note that in the atmosphere most particles are smaller (e.g., 0.1 to
322 0.3 μm) than sample particles and the chemical characteristics of ambient aerosol are not as simple as binary chemical systems
323 in the current study. Therefore, the water kinetic inhibition should be further investigated for smaller particles containing more
324 complex systems in the future.

325 **4 Conclusions**

326 Atmospheric surfactants have potential to distribute to surface, altering mixing state hence influencing aerosol
327 hygroscopicity and CCN activity. But currently direct observation of RH–dependent mixing state of aerosol containing
328 atmospheric surfactants is scarce. In this study, dynamic mixing state and phase transitions of 20 types of submicron particles
329 containing inorganic and surface–active organic constituents were directly investigated upon relative humidity (RH) cycling
330 by Environmental Scanning Electron Microscopy (ESEM).

331 Inorganic–organic core-shell morphology was found for dry deposited mixed inorganic salt–organic surfactant particles.
332 During hydration, organic shell inhibited water diffusion exposing to inorganic cores, resulting in higher deliquescence RH
333 (88.3–99.5%) of inner inorganic phase compared with pure inorganic aerosol. This was because higher RH may facilitate phase
334 transition of organic shell from solid to semisolid, raising organic viscosity thus decreasing water diffusion exposing to
335 inorganic core. Meanwhile, we directly observed obvious Ostwald ripening of NaCl, that is, the growth of larger NaCl crystal
336 at the expense of smaller ones, in 6 among 10 NaCl–organic surfactant systems. As a result of water inhibition by surfactant
337 shell, Ostwald ripening in all systems occurred at RH above 90%, which were higher than reported RH range of pure NaCl
338 measured at 27°C (75–77%).

339 During dehydration, 8 among 20 chemical systems underwent LLPS, including 4 AS–organic surfactant systems and 4
340 NaCl–organic surfactant systems. LLPS was always observed when $\text{O:C} \leq 0.4$ and never been observed when $\text{O:C} > \sim 0.57$.
341 SRH values of AS–organic surfactant particles were generally higher than SRH of corresponding NaCl–organic surfactant
342 systems, which was consistent with reported salting out efficiency of inorganic salts. OVF showed a controversial effect on
343 SRH of inorganic salt–organic surfactant systems. Additionally, inorganic salt–organic surfactant systems without LLPS

344 underwent solid phase separation after efflorescence and also showed distinct separated phases. Our results provide a
345 comprehensive and unique insights into the dynamic evolution of inorganic salt–organic surfactant particles under fluctuating
346 atmospheric conditions, which could help improve our fundamental knowledge and decrease uncertainty of model estimation
347 on global radiative effect.

348

349 **Data availability.** The experiment data are available at ZENODO (<https://doi.org/10.5281/zenodo.8079001>)

350

351 **Author contributions.** CX and BK did the experiments, analyzed data. CX plotted the figures and wrote the original draft. FZ
352 and XP contributed to discussion and reviewed the manuscript. BK and ZX reviewed the manuscript and contributed to the
353 fund acquisition. ZW administrated the project, conceptualized the study, reviewed the manuscript and contributed to fund
354 acquisition.

355

356 **Financial support.** The research was supported by National Natural Science Foundation of China (91844301, 41805100,
357 42005087, and 42005086) and the Key Research and Development Program of Zhejiang Province (2021C03165 and
358 2022C03084).

359

360 **Acknowledgment.** We thank Yuzhong Zhang from School of Engineering, Lin Liu and Wenjing Cao from Instrumentation and
361 Service Center for Physical Sciences at Westlake University for the supporting in ESEM experiments.

362

363 **Competing interests.** The authors declare no competing financial interest.

364 Reference

365 Altaf, M. B. and Freedman, M. A.: Effect of Drying Rate on Aerosol Particle Morphology, *J. Phys. Chem. Lett.*, 8,
366 3613-3618, <https://doi.org/10.1021/acs.jpcllett.7b01327>, 2017.

367 Altaf, M. B., Dutcher, D. D., Raymond, T. M., and Freedman, M. A.: Effect of Particle Morphology on Cloud
368 Condensation Nuclei Activity, *ACS Earth Space Chem.*, 2, 634-639,
369 <https://doi.org/10.1021/acsearthspacechem.7b00146>, 2018.

370 Bertram, A. K., Martin, S. T., Hanna, S. J., Smith, M. L., Bodsworth, A., Chen, Q., Kuwata, M., Liu, A., You, Y.,
371 and Zorn, S. R.: Predicting the Relative Humidities of Liquid-Liquid Phase Separation, Efflorescence, and
372 Deliquescence of Mixed Particles of Ammonium Sulfate, Organic Material, and Water Using the Organic-to-
373 Sulfate Mass Ratio of the Particle and the Oxygen-to-Carbon Elemental Ratio of the Organic Component,
374 *Atmos. Chem. Phys.*, 11, 10995-11006, <https://doi.org/10.5194/acp-11-10995-2011>, 2011.

- 375 Boistelle, R. and Astier, J. P.: Crystallization Mechanisms in Solution, *J. Cryst. Growth*, 90, 14-30,
376 [https://doi.org/10.1016/0022-0248\(88\)90294-1](https://doi.org/10.1016/0022-0248(88)90294-1), 1988.
- 377 Bruggemann, M., Xu, R. S., Tilgner, A., Kwong, K. C., Mutzel, A., Poon, H. Y., Otto, T., Schaefer, T., Poulain, L.,
378 Chan, M. N., and Herrmann, H.: Organosulfates in Ambient Aerosol: State of Knowledge and Future Research
379 Directions on Formation, Abundance, Fate, and Importance, *Environ. Sci. Technol.*, 54, 3767-3782,
380 <https://doi.org/10.1021/acs.est.9b06751>, 2020.
- 381 Cheng, M. Q. and Kuwata, M.: Development of the Low-Temperature Hygroscopicity Tandem Differential
382 Mobility Analyzer (Low-T HTDMA) and its Application to (NH₄)₂SO₄ and NaCl Particles, *J. Aerosol Sci.*,
383 168, 106111, <https://doi.org/10.1016/j.jaerosci.2022.106111>, 2023.
- 384 Choi, M. Y. and Chan, C. K.: The Effects of Organic Species on the Hygroscopic Behaviors of Inorganic Aerosols,
385 *Environ. Sci. Technol.*, 36, 2422-2428, <https://doi.org/10.1021/es0113293>, 2002.
- 386 Ciobanu, V. G., Marcolli, C., Krieger, U. K., Weers, U., and Peter, T.: Liquid-Liquid Phase Separation in Mixed
387 Organic/Inorganic Aerosol Particles, *J. Phys. Chem. A*, 113, 10966-10978, <https://doi.org/10.1021/jp905054d>,
388 2009.
- 389 Fountoukis, C. and Nenes, A.: ISORROPIA II: a computationally efficient thermodynamic equilibrium model for
390 K⁺-Ca²⁺-Mg²⁺-NH₄⁺-Na⁺-SO₄²⁻-NO₃⁻-Cl-H₂O aerosols, *Atmos. Chem. Phys.*, 7, 4639-4659,
391 <https://doi.org/10.5194/acp-7-4639-2007>, 2007.
- 392 Freedman, M. A.: Liquid-Liquid Phase Separation in Supermicrometer and Submicrometer Aerosol Particles, *Acc.*
393 *Chem. Res.*, 53, 1102-1110, <https://doi.org/10.1021/acs.accounts.0c00093>, 2020.
- 394 Ghorai, S., Wang, B. B., Tivanski, A., and Laskin, A.: Hygroscopic Properties of Internally Mixed Particles
395 Composed of NaCl and Water-Soluble Organic Acids, *Environ. Sci. Technol.*, 48, 2234-2241,
396 <https://doi.org/10.1021/es404727u>, 2014.
- 397 Griffin, R. J., Nguyen, K., Dabdub, D., and Seinfeld, J. H.: A coupled hydrophobic-hydrophilic model for predicting
398 secondary organic aerosol formation, *J. Atmos. Chem.*, 44, 171-190,
399 <https://doi.org/10.1023/A:1022436813699>, 2003.
- 400 Guo, L. Y., Peng, C., Zong, T. M., Gu, W. J., Ma, Q. X., Wu, Z. J., Wang, Z., Ding, X., Hu, M., Wang, X. M., and
401 Tang, M. J.: Comprehensive Characterization of Hygroscopic Properties of Methanesulfonates, *Atmos.*
402 *Environ.*, 224, 117349, <https://doi.org/10.1016/j.atmosenv.2020.117349>, 2020.
- 403 Ho, K. F., Lee, S. C., Ho, S. S. H., Kawamura, K., Tachibana, E., Cheng, Y., and Zhu, T.: Dicarboxylic acids,
404 ketocarboxylic acids, α -dicarbonyls, fatty acids, and benzoic acid in urban aerosols collected during the 2006

405 Campaign of Air Quality Research in Beijing (CAREBeijing-2006), *J. Geophys. Res.: Atmos.*, 115, D19312,
406 <https://doi.org/10.1029/2009jd013304>, 2010.

407 Hyder, M., Genberg, J., Sandahl, M., Swietlicki, E., and Jönsson, J. Å.: Yearly trend of dicarboxylic acids in organic
408 aerosols from south of Sweden and source attribution, *Atmos. Environ.*, 57, 197-204,
409 <https://doi.org/10.1016/j.atmosenv.2012.04.027>, 2012.

410 Kirpes, R. M., Lei, Z. Y., Fraund, M., Gunsch, M. J., May, N. W., Barrett, T. E., Moffett, C. E., Schauer, A. J.,
411 Alexander, B., Upchurch, L. M., China, S., Quinn, P. K., Moffet, R. C., Laskin, A., Sheesley, R. J., Pratt, K.
412 A., and Ault, A. P.: Solid organic-coated ammonium sulfate particles at high relative humidity in the
413 summertime Arctic atmosphere, *Proc. Natl. Acad. Sci. U.S.A.*, 119, <https://doi.org/10.1073/pnas.2104496119>,
414 2022.

415 Kwamena, N. O. A., Buajarn, J., and Reid, J. P.: Equilibrium Morphology of Mixed Organic/Inorganic/Aqueous
416 Aerosol Droplets: Investigating the Effect of Relative Humidity and Surfactants, *J. Phys. Chem. A*, 114, 5787-
417 5795, <https://doi.org/10.1021/jp1003648>, 2010.

418 Lambert, F., Kug, J. S., Park, R. J., Mahowald, N., Winckler, G., Abe-Ouchi, A., O'ishi, R., Takemura, T., and Lee,
419 J. H.: The role of mineral-dust aerosols in polar temperature amplification, *Nat. Clim. Change*, 3, 487-491,
420 <https://doi.org/10.1038/Nclimate1785>, 2013.

421 Laskin, A., Cowin, J. P., and Iedema, M. J.: Analysis of Individual Environmental Particles using Modern Methods
422 of Electron Microscopy and X-ray Microanalysis, *J. Electron. Spectrosc. Relat. Phenom.*, 150, 260-274,
423 <https://doi.org/10.1016/j.elspec.2005.06.008>, 2006.

424 Laskina, O., Morris, H. S., Grandquist, J. R., Qiu, Z., Stone, E. A., Tivanski, A. V., and Grassian, V. H.: Size Matters
425 in the Water Uptake and Hygroscopic Growth of Atmospherically Relevant Multicomponent Aerosol Particles,
426 *J. Phys. Chem. A*, 119, 4489-4497, <https://doi.org/10.1021/jp510268p>, 2015.

427 Li, W. J., Shao, L. Y., Zhang, D. Z., Ro, C. U., Hu, M., Bi, X. H., Geng, H., Matsuki, A., Niu, H. Y., and Chen, J.
428 M.: A review of single aerosol particle studies in the atmosphere of East Asia: morphology, mixing state,
429 source, and heterogeneous reactions, *J. Cleaner Prod.*, 112, 1330-1349,
430 <https://doi.org/10.1016/j.jclepro.2015.04.050>, 2016.

431 Li, W. J., Teng, X. M., Chen, X. Y., Liu, L., Xu, L., Zhang, J., Wang, Y. Y., Zhang, Y., and Shi, Z. B.: Organic
432 Coating Reduces Hygroscopic Growth of Phase-Separated Aerosol Particles, *Environ. Sci. Technol.*, 55,
433 16339-16346, <https://doi.org/10.1021/acs.est.1c05901>, 2021.

434 Ma, S. S., Pang, S. F., Li, J., and Zhang, Y. H.: A review of efflorescence kinetics studies on atmospherically relevant

435 particles, *Chemosphere*, 277, 130320, <https://doi.org/10.1016/j.chemosphere.2021.130320>, 2021.

436 Martin, S. T.: Phase Transitions of Aqueous Atmospheric Particles, *Chem. Rev.*, 100, 3403-3453,
437 <https://doi.org/10.1021/cr990034t>, 2000.

438 Metzger, S., Dentener, F., Krol, M., Jeuken, A., and Lelieveld, J.: Gas/aerosol partitioning 2. Global modeling
439 results, *Journal of Geophysical Research-Atmospheres*, 107, ACH-17, <https://doi.org/10.1029/2001jd001103>,
440 2002a.

441 Metzger, S., Dentener, F., Pandis, S., and Lelieveld, J.: Gas/aerosol partitioning 1. A computationally efficient
442 model, *Journal of Geophysical Research-Atmospheres*, 107, D16, <https://doi.org/10.1029/2001jd001102>,
443 2002b.

444 Myhre, G., Bellouin, N., Berglen, T. F., Berntsen, T. K., Boucher, O., Grini, A., Isaksen, I. S. A., Johnsrud, M.,
445 Mishchenko, M. I., Stordal, F., and Tanre, D.: Comparison of the radiative properties and direct radiative effect
446 of aerosols from a global aerosol model and remote sensing data over ocean, *Tellus B*, 59, 115-129,
447 <https://doi.org/10.1111/j.1600-0889.2006.00238.x>, 2007.

448 Nandy, L., Yao, Y., Zheng, Z. H., and Riemer, N.: Water uptake and optical properties of mixed organic-inorganic
449 particles, *Aerosol Sci. Technol.*, 55, 1398-1413, <https://doi.org/10.1080/02786826.2021.1966378>, 2021.

450 Nguyen, Q. T., Kjær, K. H., Kling, K. I., Boesen, T., and Bilde, M.: Impact of Fatty Acid Coating on the CCN
451 Activity of Sea Salt Particles, *Tellus B: Chem. Phys. Meteorol.*, 69, 1304064,
452 <https://doi.org/10.1080/16000889.2017.1304064>, 2017.

453 Noziere, B.: Don't Forget the Surface, *Science*, 351, 1396-1397, <https://doi.org/10.1126/science.aaf3253>, 2016.

454 O'Brien, R. E., Wang, B. B., Kelly, S. T., Lundt, N., You, Y., Bertram, A. K., Leone, S. R., Laskin, A., and Gilles,
455 M. K.: Liquid-Liquid Phase Separation in Aerosol Particles: Imaging at the Nanometer Scale, *Environ. Sci.*
456 *Technol.*, 49, 4995-5002, <https://doi.org/10.1021/acs.est.5b00062>, 2015.

457 Ohno, P. E., Qin, Y. M., Ye, J. H., Wang, J. F., Bertram, A. K., and Martin, S. T.: Fluorescence Aerosol Flow Tube
458 Spectroscopy to Detect Liquid-Liquid Phase Separation, *ACS Earth Space Chem.*, 5, 1223-1232,
459 <https://doi.org/10.1021/acsearthspacechem.1c00061>, 2021.

460 Ohno, P. E., Brandao, L., Rainone, E. M., Aruffo, E., Wang, J. F., Qin, Y. M., and Martin, S. T.: Size Dependence
461 of Liquid-Liquid Phase Separation by in Situ Study of Flowing Submicron Aerosol Particles, *J. Phys. Chem.*
462 *A*, 127, 2967-2974, <https://doi.org/10.1021/acs.jpca.2c08224>, 2023.

463 Onasch, T. B., Siefert, R. L., Brooks, S. D., Prenni, A. J., Murray, B., Wilson, M. A., and Tolbert, M. A.: Infrared
464 Spectroscopic Study of The Deliquescence and Efflorescence of Ammonium Sulfate Aerosol as a Function of

465 Temperature, *Journal of Geophysical Research-Atmospheres*, 104, 21317-21326,
466 <https://doi.org/10.1029/1999jd900384>, 1999.

467 Ott, E. J. E. and Freedman, M. A.: Influence of Ions on the Size Dependent Morphology of Aerosol Particles, *ACS*
468 *Earth Space Chem.*, 5, 2320-2328, <https://doi.org/10.1021/acsearthspacechem.1c00210>, 2021.

469 Ott, E. J. E., Kucinski, T. M., Dawson, J. N., and Freedman, M. A.: Use of Transmission Electron Microscopy for
470 Analysis of Aerosol Particles and Strategies for Imaging Fragile Particles, *Anal. Chem.*, 93, 11347-11356,
471 <https://doi.org/10.1021/acs.analchem.0c05225>, 2021.

472 Peng, C., Chan, M. N., and Chan, C. K.: The Hygroscopic Properties of Dicarboxylic and Multifunctional Acids:
473 Measurements and UNIFAC Predictions, *Environ. Sci. Technol.*, 35, 4495-4501,
474 <https://doi.org/10.1021/es0107531>, 2001.

475 Peng, C., Jing, B., Guo, Y. C., Zhang, Y. H., and Ge, M. F.: Hygroscopic Behavior of Multicomponent Aerosols
476 Involving NaCl and Dicarboxylic Acids, *J. Phys. Chem. A*, 120, 1029-1038,
477 <https://doi.org/10.1021/acs.jpca.5b09373>, 2016.

478 Peng, C., Chen, L., and Tang, M.: A Database for Deliquescence and Efflorescence Relative Humidities of
479 Compounds with Atmospheric Relevance, *Fundam. Res.*, 2, 578-587,
480 <https://doi.org/10.1016/j.fmre.2021.11.021>, 2022.

481 Petters, M. D. and Kreidenweis, S. M.: A single parameter representation of hygroscopic growth and cloud
482 condensation nucleus activity, *Atmos. Chem. Phys.*, 7, 1961-1971, <https://doi.org/10.5194/acp-7-1961-2007>,
483 2007.

484 Pöhlker, C., Saturno, J., Krüger, M. L., Förster, J. D., Weigand, M., Wiedemann, K. T., Bechtel, M., Artaxo, P., and
485 Andreae, M. O.: Efflorescence upon Humidification? X-ray Microspectroscopic in situ Observation of
486 Changes in Aerosol Microstructure and Phase State upon Hydration, *Geophys. Res. Lett.*, 41, 3681-3689,
487 <https://doi.org/10.1002/2014gl059409>, 2014.

488 Pöschl, U.: Atmospheric Aerosols: Composition, Transformation, Climate and Health Effects, *Angew. Chem. Int.*
489 *Ed.*, 44, 7520-7540, <https://doi.org/10.1002/anie.200501122>, 2005.

490 Posfai, M., Axisa, D., Tompa, E., Freney, E., Brientjes, R., and Buseck, P. R.: Interactions of Mineral Dust with
491 Pollution and Clouds: An Individual-Particle TEM Study of Atmospheric Aerosol from Saudi Arabia, *Atmos.*
492 *Res.*, 122, 347-361, <https://doi.org/10.1016/j.atmosres.2012.12.001>, 2013.

493 Pye, H. O. T., Murphy, B. N., Xu, L., Ng, N. L., Carlton, A. G., Guo, H. Y., Weber, R., Vasilakos, P., Appel, K. W.,
494 Budisulistiorini, S. H., Surratt, J. D., Nenes, A., Hu, W. W., Jimenez, J. L., Isaacman-VanWertz, G., Misztal,

495 P. K., and Goldstein, A. H.: On the implications of aerosol liquid water and phase separation for organic aerosol
496 mass, *Atmos. Chem. Phys.*, 17, 343-369, <https://doi.org/10.5194/acp-17-343-2017>, 2017.

497 Reed, N. W., Wing, B. A., Tolbert, M. A., and Browne, E. C.: Trace H₂S Promotes Organic Aerosol Production and
498 Organosulfur Compound Formation in Archean Analog Haze Photochemistry Experiments, *Geophys. Res.
499 Lett.*, 49, <https://doi.org/10.1029/2021GL097032>, 2022.

500 Riemer, N., Ault, A. P., West, M., Craig, R. L., and Curtis, J. H.: Aerosol Mixing State: Measurements, Modeling,
501 and Impacts, *Rev. Geophys.*, 57, 187-249, <https://doi.org/10.1029/2018rg000615>, 2019.

502 Römpp, A., Winterhalter, R., and Moortgat, G. K.: Oxodicarboxylic acids in atmospheric aerosol particles, *Atmos.
503 Environ.*, 40, 6846-6862, <https://doi.org/10.1016/j.atmosenv.2006.05.053>, 2006.

504 Roy, P., Mael, L. E., Makhnenko, I., Martz, R., Grassian, V. H., and Dutcher, C. S.: Temperature-Dependent Phase
505 Transitions of Aqueous Aerosol Droplet Systems in Microfluidic Traps, *ACS Earth Space Chem.*, 4, 1527-
506 1539, <https://doi.org/10.1021/acsearthspacechem.0c00114>, 2020.

507 Ruehl, C. R. and Wilson, K. R.: Surface Organic Monolayers Control the Hygroscopic Growth of Submicrometer
508 Particles at High Relative Humidity, *J. Phys. Chem. A*, 118, 3952-3966, <https://doi.org/10.1021/jp502844g>,
509 2014.

510 Ruehl, C. R., Davies, J. F., and Wilson, K. R.: An Interfacial Mechanism for Cloud Droplet Formation on Organic
511 Aerosols, *Science*, 351, 1447-1450, <https://doi.org/10.1126/science.aad4889>, 2016.

512 Shiraiwa, M., Zuend, A., Bertram, A. K., and Seinfeld, J. H.: Gas-Particle Partitioning of Atmospheric Aerosols:
513 Interplay of Physical State, Non-Ideal Mixing and Morphology, *Physical Chemistry Chemical Physics*, 15,
514 11441-11453, <https://doi.org/10.1039/c3cp51595h>, 2013.

515 Song, M., Marcolli, C., Krieger, U. K., Zuend, A., and Peter, T.: Liquid-Liquid Phase Separation and Morphology
516 of Internally Mixed Dicarboxylic Acids/Ammonium Sulfate/Water Particles, *Atmos. Chem. Phys.*, 12, 2691-
517 2712, <https://doi.org/10.5194/acp-12-2691-2012>, 2012a.

518 Song, M., Marcolli, C., Krieger, U. K., Zuend, A., and Peter, T.: Liquid-Liquid Phase Separation in Aerosol Particles:
519 Dependence on O:C, Organic Functionalities, and Compositional Complexity, *Geophys. Res. Lett.*, 39,
520 L19801, <https://doi.org/10.1029/2012gl052807>, 2012b.

521 Song, M., Maclean, A. M., Huang, Y. Z., Smith, N. R., Blair, S. L., Laskin, J., Laskin, A., DeRieux, W. S. W., Li,
522 Y., Shiraiwa, M., Nizkorodov, S. A., and Bertram, A. K.: Liquid-Liquid Phase Separation and Viscosity within
523 Secondary Organic Aerosol Generated from Diesel Fuel Vapors, *Atmos. Chem. Phys.*, 19, 12515-12529,
524 <https://doi.org/10.5194/acp-19-12515-2019>, 2019.

525 Song, M. J., Liu, P. F., Martin, S. T., and Bertram, A. K.: Liquid-Liquid Phase Separation in Particles Containing
526 Secondary Organic Material Free of Inorganic Salts, *Atmos. Chem. Phys.*, 17, 11261-11271,
527 <https://doi.org/10.5194/acp-17-11261-2017>, 2017.

528 Stewart, D. J., Cai, C., Naylor, J., Preston, T. C., Reid, J. P., Krieger, U. K., Marcolli, C., and Zhang, Y. H.: Liquid-
529 Liquid Phase Separation in Mixed Organic/Inorganic Single Aqueous Aerosol Droplets, *J. Phys. Chem. A*, 119,
530 4177-4190, <https://doi.org/10.1021/acs.jpca.5b01658>, 2015.

531 Takahama, S., Pathak, R. K., and Pandis, S. N.: Efflorescence Transitions of Ammonium Sulfate Particles Coated
532 with Secondary Organic Aerosol, *Environ. Sci. Technol.*, 41, 2289-2295, <https://doi.org/10.1021/es0619915>,
533 2007.

534 Ting, Y. C., Mitchell, E. J. S., Allan, J. D., Liu, D. T., Spracklen, D. V., Williams, A., Jones, J. M., Lea-Langton, A.
535 R., McFiggans, G., and Coe, H.: Mixing State of Carbonaceous Aerosols of Primary Emissions from
536 "Improved" African Cookstoves, *Environ. Sci. Technol.*, 52, 10134-10143,
537 <https://doi.org/10.1021/acs.est.8b00456>, 2018.

538 Tolocka, M. P. and Turpin, B.: Contribution of Organosulfur Compounds to Organic Aerosol Mass, *Environ. Sci.*
539 *Technol.*, 46, 7978-7983, <https://doi.org/10.1021/es300651v>, 2012.

540 Tong, Y. K., Meng, X. X. Y., Zhou, B., Sun, R., Wu, Z. J., Hu, M., and Ye, A. P.: Detecting the pH-dependent liquid-
541 liquid phase separation of single levitated aerosol microdroplets via laser tweezers-Raman spectroscopy, *Front.*
542 *Phys.*, 10, <https://doi.org/10.3389/fphy.2022.969921>, 2022.

543 Unga, F., Choel, M., Derimian, Y., Deboudt, K., Dubovik, O., and Goloub, P.: Microscopic Observations of Core-
544 Shell Particle Structure and Implications for Atmospheric Aerosol Remote Sensing, *Journal of Geophysical*
545 *Research-Atmospheres*, 123, 13944-13962, <https://doi.org/10.1029/2018jd028602>, 2018.

546 Veghte, D. P., Bittner, D. R., and Freedman, M. A.: Cryo-Transmission Electron Microscopy Imaging of the
547 Morphology of Submicrometer Aerosol Containing Organic Acids and Ammonium Sulfate, *Anal. Chem.*, 86,
548 2436-2442, <https://doi.org/10.1021/ac403279f>, 2014.

549 Voorhees, P. W.: The Theory of Ostwald Ripening, *J. Stat. Phys.*, 38, 231-252, <https://doi.org/10.1007/Bf01017860>,
550 1985.

551 Wang, N., Jing, B., Wang, P., Wang, Z., Li, J. R., Pang, S. F., Zhang, Y. H., and Ge, M. F.: Hygroscopicity and
552 Compositional Evolution of Atmospheric Aerosols Containing Water-Soluble Carboxylic Acid Salts and
553 Ammonium Sulfate: Influence of Ammonium Depletion, *Environ. Sci. Technol.*, 53, 6225-6234,
554 <https://doi.org/10.1021/acs.est.8b07052>, 2019.

555 Wang, W. H., Shao, L. Y., Mazzoleni, C., Li, Y. W., Kotthaus, S., Grimmond, S., Bhandari, J., Xing, J. P., Feng, X.
556 L., Zhang, M. Y., and Shi, Z. B.: Measurement report: Comparison of wintertime individual particles at ground
557 level and above the mixed layer in urban Beijing, *Atmos. Chem. Phys.*, 21, 5301-5314,
558 <https://doi.org/10.5194/acp-21-5301-2021>, 2021.

559 Wise, M. E., Martin, S. T., Russell, L. M., and Buseck, P. R.: Water Uptake by NaCl Particles Prior to Deliquescence
560 and the Phase Rule, *Aerosol Sci. Technol.*, 42, 281-294, <https://doi.org/10.1080/02786820802047115>, 2008.

561 Xiong, C., Chen, X. Y., Ding, X. L., Kuang, B. Y., Pei, X. Y., Xu, Z. N., Yang, S. K., Hu, H., and Wang, Z. B.:
562 Reconsideration of Surface Tension and Phase State Effects on Cloud Condensation Nuclei Activity Based on
563 the Atomic Force Microscopy Measurement, *Atmos. Chem. Phys.*, 22, 16123-16135,
564 <https://doi.org/10.5194/acp-22-16123-2022>, 2022.

565 Xu, L., Fukushima, S., Sobanska, S., Murata, K., Naganuma, A., Liu, L., Wang, Y. Y., Niu, H. Y., Shi, Z. B., Kojima,
566 T., Zhang, D. Z., and Li, W. J.: Tracing the evolution of morphology and mixing state of soot particles along
567 with the movement of an Asian dust storm, *Atmos. Chem. Phys.*, 20, 14321-14332,
568 <https://doi.org/10.5194/acp-20-14321-2020>, 2020.

569 Xu, W. Q., Chen, C., Qiu, Y. M., Li, Y., Zhang, Z. Q., Karnezi, E., Pandis, S. N., Xie, C. H., Li, Z. J., Sun, J. X.,
570 Ma, N., Xu, W. Y., Fu, P. Q., Wang, Z. F., Zhu, J., Worsnop, D. R., Ng, N. L., and Sun, Y. L.: Organic aerosol
571 volatility and viscosity in the North China Plain: contrast between summer and winter, *Atmos. Chem. Phys.*,
572 21, 5463-5476, <https://doi.org/10.5194/acp-21-5463-2021>, 2021.

573 Yang, H., Wang, N., Pang, S. F., Zheng, C. M., and Zhang, Y. H.: Chemical reaction between sodium pyruvate and
574 ammonium sulfate in aerosol particles and resultant sodium sulfate efflorescence, *Chemosphere*, 215, 554-
575 562, <https://doi.org/10.1016/j.chemosphere.2018.10.062>, 2019.

576 You, Y., Renbaum-Wolff, L., Carreras-Sospedra, M., Hanna, S. J., Hiranuma, N., Kamal, S., Smith, M. L., Zhang,
577 X. L., Weber, R. J., Shilling, J. E., Dabdub, D., Martin, S. T., and Bertram, A. K.: Images Reveal that
578 Atmospheric Particles can Undergo Liquid-Liquid Phase Separations, *Proc. Natl. Acad. Sci. U.S.A.*, 109,
579 13188-13193, <https://doi.org/10.1073/pnas.1206414109>, 2012.

580 You, Y., Renbaum-Wolff, L., and Bertram, A. K.: Liquid-liquid phase separation in particles containing organics
581 mixed with ammonium sulfate, ammonium bisulfate, ammonium nitrate or sodium chloride, *Atmos. Chem.*
582 *Phys.*, 13, 11723-11734, <https://doi.org/10.5194/acp-13-11723-2013>, 2013.

583 You, Y. and Bertram, A. K.: Effects of Molecular Weight and Temperature on Liquid-Liquid Phase Separation in
584 Particles Containing Organic Species and Inorganic Salts, *Atmos. Chem. Phys.*, 15, 1351-1365,

585 <https://doi.org/10.5194/acp-15-1351-2015>, 2015.

586 Zavacka, K., Nedela, V., Olbert, M., Tihlarikova, E., Vetrakova, L., Yang, X., and Heger, D.: Temperature and
587 Concentration Affect Particle Size Upon Sublimation of Saline Ice: Implications for Sea Salt Aerosol
588 Production in Polar Regions, *Geophys. Res. Lett.*, 49, <https://doi.org/10.1029/2021GL097098>, 2022.

589 Zaveri, R. A., Easter, R. C., Fast, J. D., and Peters, L. K.: Model for Simulating Aerosol Interactions and Chemistry
590 (MOSAIC), *Journal of Geophysical Research-Atmospheres*, 113, D13204,
591 <https://doi.org/10.1029/2007jd008782>, 2008.

592 Zeng, G., Kelley, J., Kish, J. D., and Liu, Y.: Temperature-Dependent Deliquescent and Efflorescent Properties of
593 Methanesulfonate Sodium Studied by ATR-FTIR Spectroscopy, *J. Phys. Chem. A*, 118, 583-591,
594 <https://doi.org/10.1021/jp405896y>, 2014.

595 Zhang, J., Yuan, Q., Liu, L., Wang, Y. Y., Zhang, Y. X., Xu, L., Pang, Y., Zhu, Y. H., Niu, H. Y., Shao, L. Y., Yang,
596 S. S., Liu, H., Pan, X. L., Shi, Z. B., Hu, M., Fu, P. Q., and Li, W. J.: Trans-Regional Transport of Haze
597 Particles From the North China Plain to Yangtze River Delta During Winter, *Journal of Geophysical Research-*
598 *Atmospheres*, 126, <https://doi.org/10.1029/2020JD033778>, 2021.

599 Zhang, J., Wang, Y. Y., Teng, X. M., Liu, L., Xu, Y. S., Ren, L. H., Shi, Z. B., Zhang, Y., Jiang, J. K., Liu, D. T., Hu,
600 M., Shao, L. Y., Chen, J. M., Martin, S. T., Zhang, X. Y., and Li, W. J.: Liquid-Liquid Phase Separation Reduces
601 Radiative Absorption by Aged Black Carbon Aerosols, *Commun. Earth Environ.*, 3, 128,
602 <https://doi.org/10.1038/s43247-022-00462-1>, 2022.

603 Zhang, Y., Chen, Y. Z., Lambe, A. T., Olson, N. E., Lei, Z. Y., Craig, R. L., Zhang, Z. F., Gold, A., Onasch, T. B.,
604 Jayne, J. T., Worsnop, D. R., Gaston, C. J., Thornton, J. A., Vizuete, W., Ault, A. P., and Surratt, J. D.: Effect
605 of the Aerosol-Phase State on Secondary Organic Aerosol Formation from the Reactive Uptake of Isoprene-
606 Derived Epoxydiols (IEPDX), *Environ. Sci. Technol. Lett.*, 5, 167-174,
607 <https://doi.org/10.1021/acs.estlett.8b00044>, 2018.

608 Zhang, Y. X., Zhang, Q., Yao, Z. L., and Li, H. Y.: Particle Size and Mixing State of Freshly Emitted Black Carbon
609 from Different Combustion Sources in China, *Environ. Sci. Technol.*, 54, 7766-7774,
610 <https://doi.org/10.1021/acs.est.9b07373>, 2020.

611 Zhu, Y., Pang, S., and Zhang, Y.: Observations on the unique phase transitions of inorganics relevant due to gluconic
612 acid in particles, *Atmos. Environ.*, 288, 119313, <https://doi.org/10.1016/j.atmosenv.2022.119313>, 2022.

613